Materials and Design 191 (2020) 108669

Contents lists available at ScienceDirect

Materials and Design

journal homepage: www.elsevier.com/locate/matdes

Spider silk binder for Si-based anode in lithium-ion batteries

DongWoong Choi, Kwang Leong Choy *

UCL Institute for Materials Discovery, University College London, WC1E, 7JE, United Kingdom

HIGHLIGHTS

- This is a novel approach of using natural spider silk as the effective binder material.
- The spider silk based electrodes with various weight ratios exhibited superior cyclic stability at 250 mA·g^{-1}.
- The enhanced cycling property was demonstrated through cyclic voltammetry, impedance, and performance tests.
- Such superior performance of the cell with spider silk binder might be attributed by the unique properties of silk.

GRAPHICAL ABSTRACT

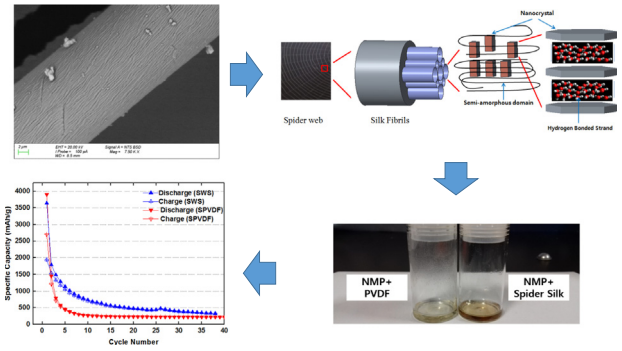

ARTICLE INFO

Article history:
Received 6 August 2019
Received in revised form 20 March 2020
Accepted 20 March 2020
Available online 21 March 2020

Keywords:
Spider silk
Silicon
Binder
Anode
Batteries
Lithium

ABSTRACT

Silicon (Si) has attracted attention for use in lithium ion batteries due to its high theoretical capacity and its natural abundance. However, significant change in the volume of Si electrodes during repeated cycles causes dramatic capacity degradation and reduces the benefits of its attractive qualities. Here, it is reported for the first time that a derivative of natural spider silk is effective for retaining the capacity and decreasing the volume expansion of Si for use in Li-ion batteries as electrodes. Relative to the Si-electrode with polyvinylidene fluoride (SPVDF), the Si-electrode containing binder with the dissolved spider silk (SWS) cells achieved significant enhanced capacities with cycling stability during repeated cycles. The SWS electrode at 250 mA g $^{-1}$ showed the discharge/charge capacities of 3642/1938 mAh g^{-1} at 1st cycle, 1789/1541 mAh g^{-1} at 2nd cycle and then reduced to 1142/1054 mAh g^{-1} at the 5th cycle. However, the capacities of the SPVDF electrode were 3903/2694 mAh g^{-1}, 1455/1211 mAh g^{-1}, and 458/435 mAh g^{-1}. Furthermore, the discharge capacity of SWS was 333 mAh g^{-1} at the 38th cycle, but that of SPVDF showed 323 mAh g^{-1} at the 7th cycle. Such superior performance with good cycling ability may be attributed to the unique properties of spider silk: the folded crystal layer with semi-amorphous structure, the superior properties of viscosity and adhesion, and the close stacking by the protein blocks as well as the side chain R-group of crystal β-sheet. The combination of these characteristics was able to restrain the deleterious change in the volume of Si materials substantially, and to provide superior electrochemical characteristics of lithium ions.

1. Introduction

Recently, there is a rapid development of battery technology with increased capacity, power, and life span. However, commercial lithium ion batteries exhibit a number of limitations. In particularly, the use of

* Corresponding author.
E-mail address: k.choy@ucl.ac.uk (K.L. Choy).

https://doi.org/10.1016/j.matdes.2020.108669

graphite anode has low capacity. Among the candidate materials to replace graphite, silicon (Si) has attracted great attention as a promising anode material that might overcome the limitation. One of the reasons is that the theoretical capacity of Si is over ten times greater than that of graphite materials. In addition, Si is both cheap and abundant which provides potential significant cost-savings for mass production. Despite these advantages, the use of Si has a number of drawbacks: large volume change of Si during repeated cycles [1], low electrical conductivity (1000 S/m) [2,3], and the formation of unstable solid electrolyte interphase (SEI) layers [4]. Among these issues, the biggest barrier to commercial application is the drastic volume expansion (3–4 times). This pulverizes the electrode material, leading to increased impedance from the loss of contact between electrode and electrolyte, and a rapid decrease in capacity [5]. Several studies have been attempted to address this through the modification of Si-embedded electrode structure to produce various morphologies. These include Si sponges [6], amorphous and crystalline Si structures [7], nanowires [8], shells [9], and hierarchical Si morphologies [10]. However, there are relatively limited studies on binder materials to reduce the dramatic volume change of Si, and investigation on the role of adhesion between active materials and conducting carbon materials.

Binders play an important role in the electrochemical performance of the electrodes. They can mechanically stabilize the electrodes during repeated cycles [11]. When lithium ions are inserted and extracted, the active material expands and contracts, respectively in the (001) direction. This weakens the interfacial contact between active and conductive materials, and causes an increase in the resistivity. Eventually, the active and conductive materials peel off from the electrode surface, which leads to a dramatic performance degradation. Therefore, the efficient use of binder and the development of better binder materials to improve mechanical stability will greatly improve battery performance and lifetime. The instability-to-weight ratio of Si is much higher than that of graphite, thus, the role of binders in Si-battery research is much more important than for graphite. The adhesive property of a binder directly affects the mechanical stabilization [12,13]. Recent binder research has focused on four main targets: adhesion strength, elasticity, cost, and environmental consideration [14]. Increasing adhesion between binders, conductive materials, and active materials [15] leads to a reduction in resistance and enhanced capacity retention. High elasticity enables large volume change of active materials during the intercalation and deintercalation of lithium-ions without performance degradation [16]. Low cost and eco-friendly materials provide a competitive edge for lithium-ions batteries (LIBs) as compared to other battery types [17].

There are various polymers that can be used as binders, such as polyvinylidene fluoride (PVDF) [14], styrene butadiene rubber (SBR)/carboxymethyl cellulose (CMC) [18], and polytetrafluoro ethylene (PTFE) [19], however, these binders have limited capability for reducing the volume change of Si electrode materials. Furthermore, by comparison to the research on many materials for use as negative and positive electrodes, only a few novel materials have been studied so far for use of binders. These include polyacrylic acid (PAA) [18], chitosan [20], and sodium-alginate [21]. For these reasons, this work focuses on the development of novel binder materials, and in particularly, nature inspired spider silk. Among these binder materials, the PVDF binder was chosen to compare with our proposed novel silk binder in this paper.

Spider silk is produced by spiders to construct webs, capture prey, to fly, and to provide protective cover [22], and its structure and function have been explained in reference [23]. The spider silk is 5 times stronger than the steel and 1000 times thinner than a human hair [24]. The silk morphology, and its chemical structure are presented in Fig. 2. The silk consists of a core of silk fibrils composed of nanocrystal sheets and semi-amorphous regions inside a silk skin. The nanocrystal sheets are crystalline β-sheets and contribute to the high tensile strength of the fibers [25]. A fiber forms cross-linked amino acid sequences, with repetition of mainly alanine or glycine. The abundant amino acids are closely packed together, providing the high strength of spider silk. The semi-amorphous regions are composed of β-spirals, and resulted in high elasticity, which enables the retention of struggling prey [25]. Each nanocrystal beta-sheet is connected with the strands by many hydrogen bonds. The hydrogen bond is known as the strongest type of intermolecular bond [26], and is usually formed in organic materials such as DNA and proteins. Along chains or sheets of proteins, there may be millions of hydrogen bonds binding each protein to its neighbour, hereby dramatically increasing the strength of the overall structure [27].

Given these unique properties of spider silk, it is hypothesized that its use as a binder may increase the packing density of active materials in battery anode; and significantly reduce the volume cyclical change associated with Si anode materials, thereby dramatically improving battery life. The aim of this article is to evaluate and establish the possibility of using spider silk solution as the binder material. This is the first study to explore the use of nature inspired spider silks as a novel binder for metal anode materials. This novel approach using spider silk provides new insights for the development advanced LIB-materials using such new binder based on spider silk to overcome the limitations of commercial binder PVDF, thus enabling a fresh assessment of volume-change issues. The design and use of spider silk will also be relevant to other energy storage applications such as supercapacitors and renewable energy devices like thermoelectrics.

2. Experimental

Natural spider silk was harvested, and immersed in *n*-methylpyrrolidone (NMP) solvent to dissolve it. The resultant solution was mixed for two weeks, and the color of the solution was observed to change from light green to dark brown during this period. Powder X-ray diffraction (XRD) was performed using a STOE STADI-P device with a Mo-Kα1 (Fig. 1) and Cu-Kα1 (Fig. 2) X-ray sources. Scanning electron microscopy (SEM, Zeiss EVO MA) was used to characterize the nanostructure and morphology. Fourier Transform Infrared Spectroscopy (FTIR) was performed using a Spectra Two (Perkin Elmer) over a wave number range of 4000 to 400 cm^{-1}, and attenuated total reflectance mode was applied in order to examine the bonding structure of each sample. The viscosity of the polyvinylidene fluoride (PVDF), and spider silk solution samples were measured using a Viscolite 700 Portable Viscometer. Each sample was measured three times and the averaged value was recorded. Contact angle analysis (Theta Auto One Attension) was performed in order to characterize the surface energy characteristics of each electrode with a different binder material. Atomic force microscopy (AFM) with an indentation tip was used to probe the physical surface. A Dimension Edge (Bruker) was used for the dimensional analysis of the silk fibers. The electrochemical performance of the Si powders (Sigma-Aldrich) was measured using a CR2032 half-cell. The negative-electrode slurries were made using a mixture of materials consisting of carbon black (super P, TIMCAL), Si, carbon black, and binder (PVDF or spider silk) with *n*-methyl pyrrolidone (NMP) as the solvent. The weight ratios of Si, carbon black, and binder material were 8:1.5:0.5 and 4.5:4.5:1, respectively. These viscous slurries were cast using an automatic casting coater on the current collectors (Cu-foil) and were dried in a vacuum oven at 80 °C for 12 h. The mass loading of Si in each electrode was provided in the Fig. 10. Li foil was used as the counter and reference electrodes. The electrolyte was a solution of 1 M $LiPF_6$ in a 1:1 volume ratio of ethyl carbonate and dimethylcarbonate, and a glass fiber separator was applied. Cells were fabricated in a glove box filled with argon gas where moisture and O_2 levels were controlled to below 0.5 ppm. Galvanostatic charge/discharge tests were performed using a Maccor system within the potential range 0.005–2.0 V (vs. Li/Li^+) at a high current density of 250 $mA \cdot g^{-1}$. Cyclic voltammetry (CV) and electrochemical impedance spectra (EIS) were performed using an Autolab system. The CV was tested in the voltage range of 0.005–2.0 V at a scan rate of 0.1 $mV \cdot s^{-1}$, and the impedance tests were carried out by applying AC

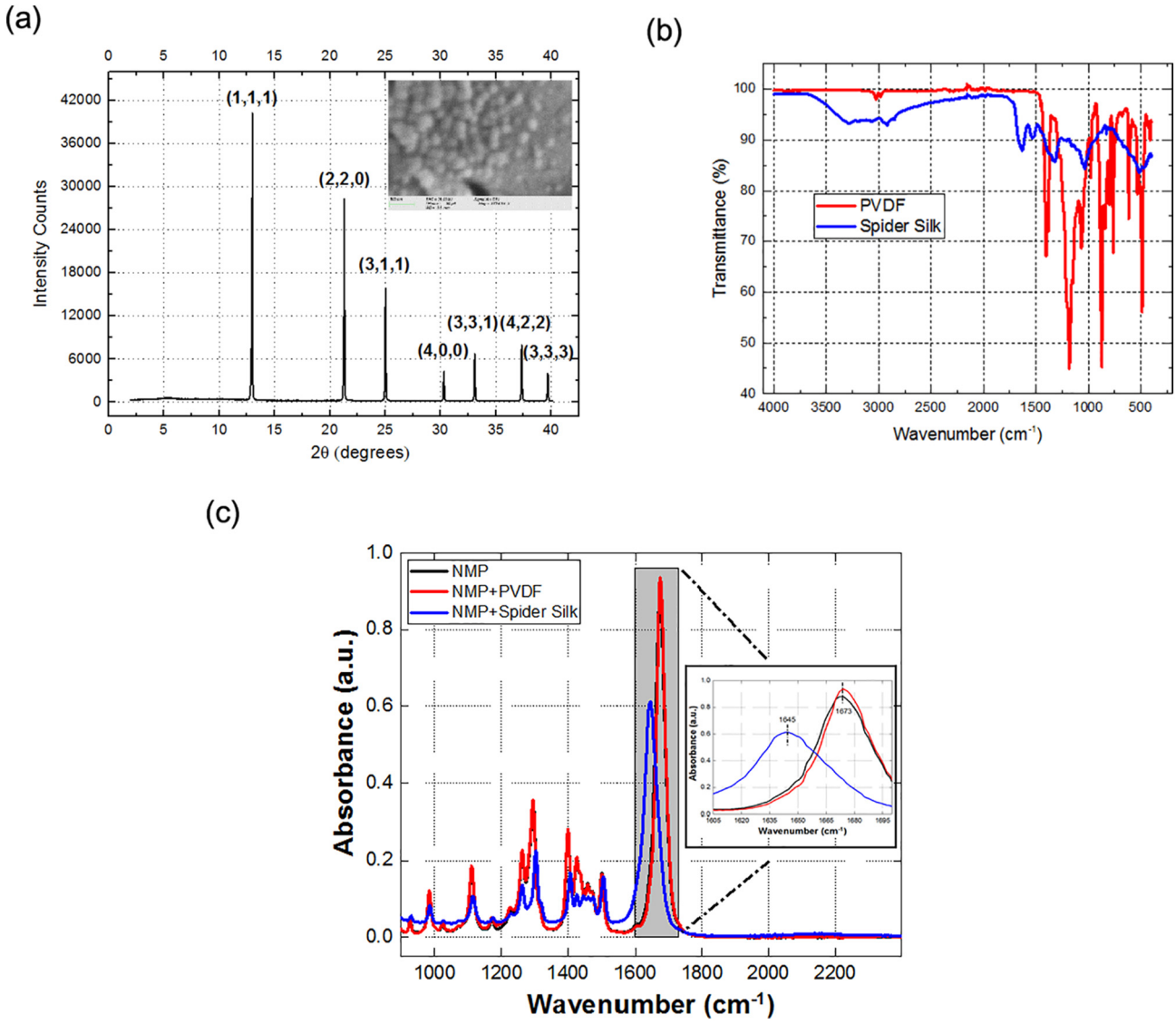

Fig. 1. (a) XRD and (inset) SEM image (the enlarged SEM image is presented in the SI Fig. 1) of Si; (b) ATR-FTIR spectra of PVDF and spider silk; (c) ATR-FTIR spectra of the liquid samples of NMP, NMP + PVDF and NMP + Spider Silk.

voltage of 10 mV over a frequency range from 10^{-1} to 10^{5} Hz. The Si-LIB with PVDF or spider silk binder was denoted as SPVDF or SWS, respectively.

3. Results and discussions

XRD (Mo-Kα1 radiation) and SEM were used to analyze the crystal structure and morphology of the Si-materials. The results are shown in Fig. 1(a). XRD confirms the powders are Si with quartz crystal structure with no apparent impurity (PDF #27-1402) present. The scanning electron micrograph in Fig. 1(a) reveals the powders to be mostly nanoparticulates (see the inset image in Fig. 1 (a) and SI-Fig. 1). Fig. 1(b) shows ATR-FTIR results in order to establish the bonding in PVDF and spider silk. (b). The absorption bands of PVDF are observed between 1402 and 486 cm^{-1} [28] with the absorption peaks at 486, 614, and 762 attributed to the CF_2 bending mode, and the peak at 872 cm^{-1} assigned to the CH out-of-plane deformation band. The bands at 974 and 1182 cm^{-1} indicated a CH_2 twisting mode and CF_2 symmetric stretching mode, respectively, and these presented in the polymer phase [28,29]. In the spider silk curve, bands between 3500 and 3200 cm^{-1} are originated from the NH- [30] and OH– stretching vibrations [31]. The band at 2920 cm^{-1} indicating the presence of CH stretching bond [32], and the bands at 1520 and 1318 cm^{-1} correspond to amide II and amide III groups, respectively. The band at 1628 cm^{-1} is related to amide I, and also attributed to the hydrogen bonding to the conform backbone, to connect the main chain and subgroups, and to enable longer bonds [31]. This band region indicates the L-alanylglycine, L-alanine, and glycine-rich regions [33]. Such strong hydrogen bonding interactions at high wave numbers and in the amide band regions in the ATR-FTIR spectrum of SWS are not observed in the spectrum of anode using PVDF binder, which might contribute to the use of spider silk to hinder the volume change of Si-based electrodes, thus enhancing their stability. The ATR-FTIR spectrum was also performed in order to compare each peak of three liquid samples (NMP, PVDF dissolved by NMP, spider silk dissolved by NMP). These results were presented in Fig. 1(c). The unique NMP band was observed at 1673 cm^{-1}, and this band was not moved when the PVDF was added. However, when the silk was dissolved by NMP, the band was shifted to the left at 1645 cm^{-1}. This shifting could be explained

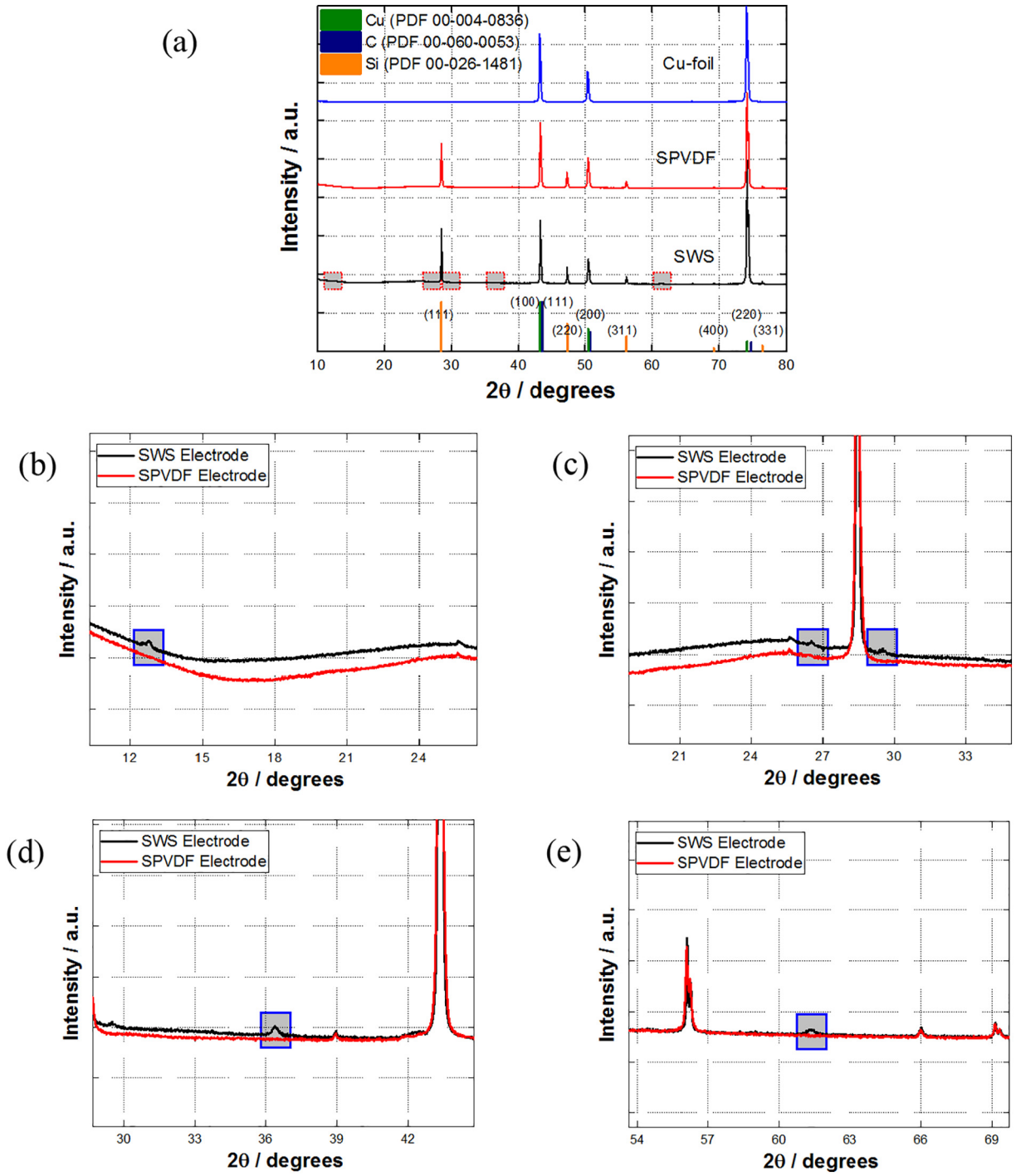

Fig. 2. (a) X-ray powder diffraction patterns of the NMP casted Cu-foil, the SWS electrode, the SPVDF electrode and the ICDD databases of Si, C, and Cu; (b–e) the unique peaks of the SWS electrode.

by the effect of crystal-beta sheet of which band is normally detected at circa. 1625–1640 cm^{-1} between 1600 and 1700 cm^{-1} of amide I band [22,34]. This could be analyzed as the structure has little changed, however, the crystal beta sheet is still in the spider silk solution (spider silk dissolved by NMP).

X-ray diffraction characterization (XRD, Cu-Kα1 radiation) was performed on three samples (i.e. NMP cast Cu-foil, the SPVDF electrode (on Cu-foil), and the SWS electrode (on Cu-foil)) in order to verify the unique crystal structure of SWS as compared to other samples. Fig. 2 (a) shows the XRD patterns of these three samples as compared with the International Centre for Diffraction Data (ICDD) databases of copper, carbon, and silicon. Fig. 2(b, c, d, e) confirmed the presence of the unique peaks of the SWS electrode. The NMP cast on Cu-foil sample was used as the control group to compare the experimental groups of SWS and SPVDF. The SWS and SPVDF samples exhibited all peaks for the silicon of the active material, the super P carbon of conductive agent, and the copper foil of current collector based on the ICDD databases. Five peaks at '2 Theta = 12.8, 26.5, 29.5, 36.4, and 61.3' were observed for the SWS. Except five unique peaks of the SWS, the others were matched well with all peaks of the SPVDF. It indicated that the

unique peaks presence in SWS were not observed in SPVDF. The five unique peaks of the SWS may be related to the unique material properties of spider silk, including the crystal beta sheet structures. The XRD results provided the direct evidence that the special structure of the spider silk in the SWS electrode, resulting enhancing electrochemical properties.

Fig. 3(a) and (b) shows SEM images of pristine spider silk exhibiting directional silk strand structure, and more images of spider silks are provided in SI-Fig. 2. Fig. 3(b) is the enlarged image of the red square area in Fig. 3(a). Fig. 3(c) is the schematic structure of a spider silk web. One silk strand consists of many silk fibrils consisting of long sequences of a protein (with glycine, one type of amino acid), and has the unique "flexible spring" structure, attached to alanine-blocks on both sides [35]. The protein of alanine has the structure of corrugated sheets, enabling them to pack closely together to form rigid blocks [27]. When a force is applied, the glycine enables stretching of the silk fibers due to its elastic and tensile behaviors, and the firm alanine blocks play the role of molecular anchoring. The optimal combination of these unique properties enables silk fibers to be both stretchable and strong, leading to ultra-tough materials.

In order to examine the surface, quantify stiffness, and adhesive strength of the spider silk, AFM was performed with the results shown in Fig. 4. Spider silk fibers were imaged on a substrate, and indicate the 3-dimensional topographical fiber pattern (a) and sample of spider silk (inset), the 2-densional fiber pattern (b), and DMT (Derjaguin-Muller-Toporov) modulus (c), adhesive strength (d) respectively. From images (a) and (b), the height of a bundle silk fiber is determined to be circa. 360 nm. The DMT image (c) is used to establish the Young's modulus. The values of Young's modulus are within the range −25.5–59.5 GPa (Note: negative and positive symbols indicate when it is compressed and stretched, respectively). As compared to the values (between 0.2 and 1.4 GPa) of Young's modulus for PVDF these values indicated much greater stiffness [21]. The images (d) presented the adhesive strength of the spider silk fiber which is within the range from 10.5 to 94.3 nN as compared to PVDF which has a typical value of circa. 5 nN [37]. The high stiffness and adhesive characteristics of spider silk would suggest that as a binder it may be able to embrace the volume expansion of the active materials while retaining rigid as compared to the conventional PVDF binder. Additional mechanical tests (e.g. peel force test and tensile test) could be performed in order to discuss and elucidate further the mechanism performance.

The samples were immersed in NMP solution in order to investigate and compare the viscosity of the binders. Fig. 5(b) showed the viscosity of these samples. The values of Viscosity per weight of PVDF and spider silk were measured to be 1303.3 and 425 cP/g, respectively, indicating that spider silk has viscosity circa. three times higher than PVDF and appeared to have a darker color as shown in Fig. 5(a). The result might be related to the higher viscosity in SWS based Si-electrode as compared to those using PVDF as the binder, which provided a good electronic contact and conduction, thus enhanced the diffusion rates of lithium ions in the electrolyte, and helped to maintain a shorter Li-insertion distances.

In order to investigate the surface properties of the binders, the contact angle was measured (see Fig. 6). The water contact angle is significantly lower for the SWS electrode (35–36°) as compared to the SPVDF electrode (75–76°). This implied that SWS is much more hydrophilic than SPVDF, and thus would have a better wetting ability with the electrolyte solvent.

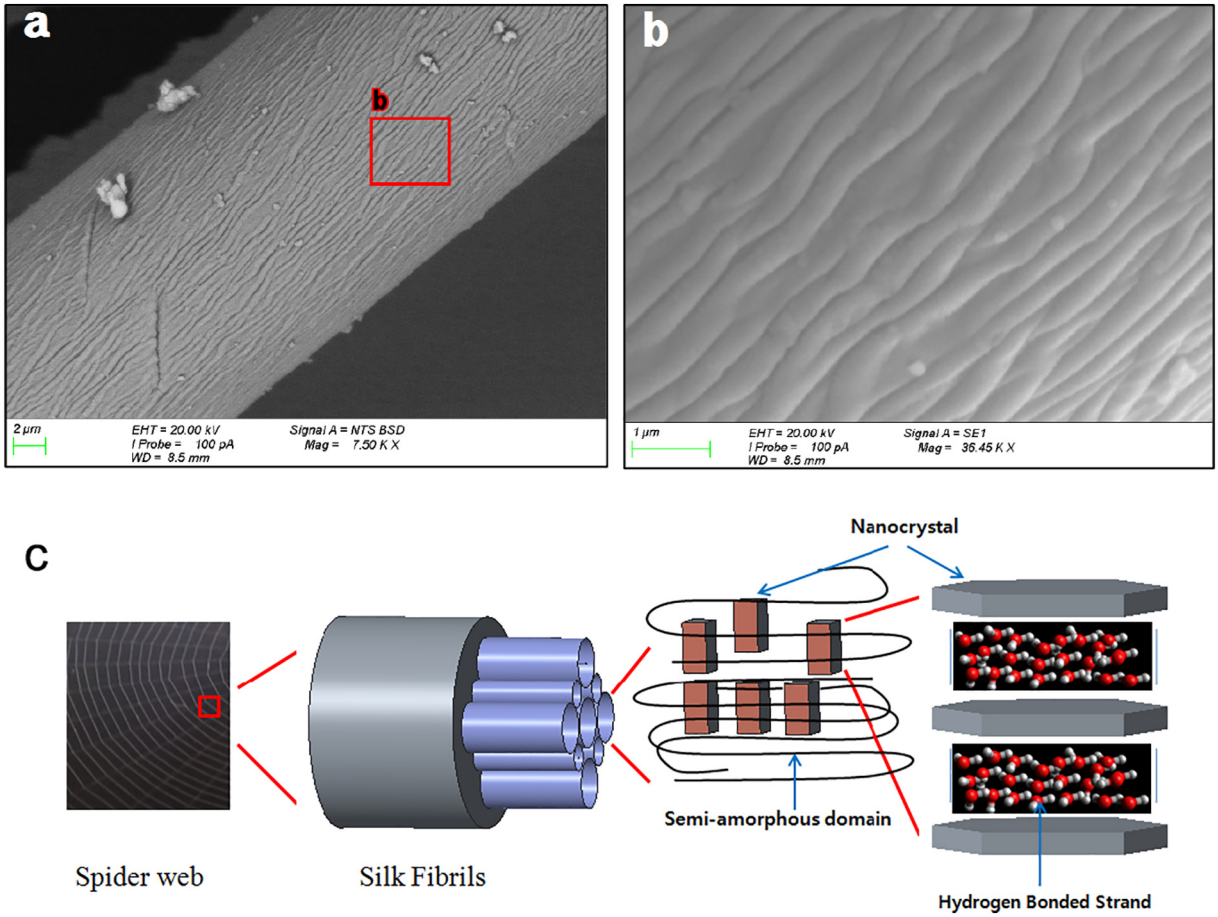

Fig. 3. SEM images; (a) a major silk holding a web; (b) the enlargement of image (a); (c) schematic structure of spider silk (adapted from the reference) [36].

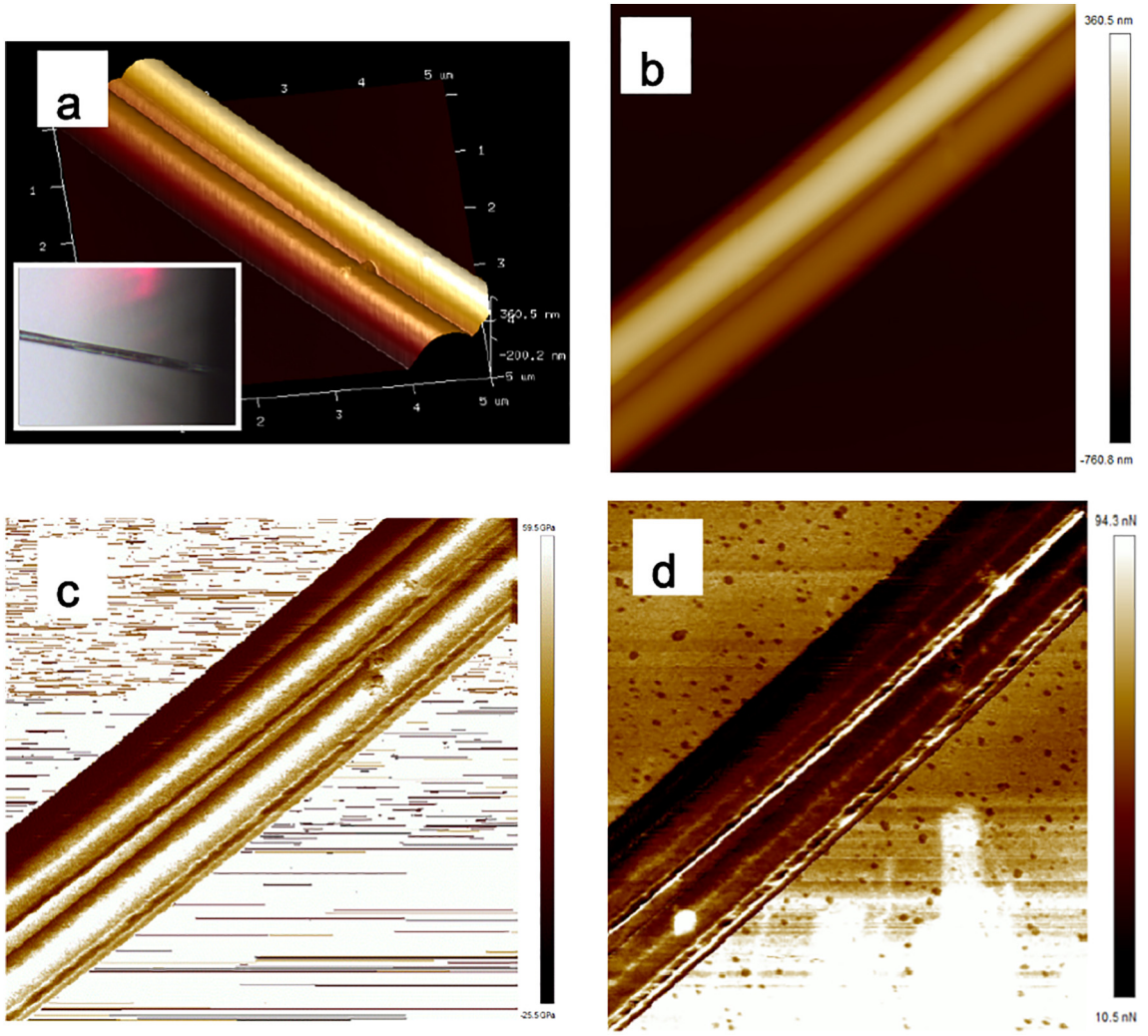

Fig. 4. (a) AFM topographical image of a 3-dimensional silk fiber and (inset) an optical image of a bundle silk fiber; (b) fiber diameter; (c) DMT modulus; and (d) adhesive strength.

The characteristics of SWS and SPVDF electrodes when exposed to fluorescent lamp was captured using a camera in order to analyze the physical and surface characteristics of each electrode. The materials in these electrodes were the same, except that the binder materials were different (spider silk solution or PVDF solution). The camera images were recorded as a short video file, and a schematic representation is shown in Fig. 7. Electrodes of SPVDF or SWS are placed on the left- or the right- hand side in Fig. 7(a), respectively. When the camera was moved across the electrodes under a fluorescent lamp, the SWS surface twinkled while those on the SPVDF did not. The reason for the twinkling of the SWS surface is that structural components in the spider silk fibrils (crystal β-sheet)would reflect the light. This result may indicates the existence of crystal β-sheet on the SWS surface in addition to the semi-amorphous domain in Fig. 3(c).

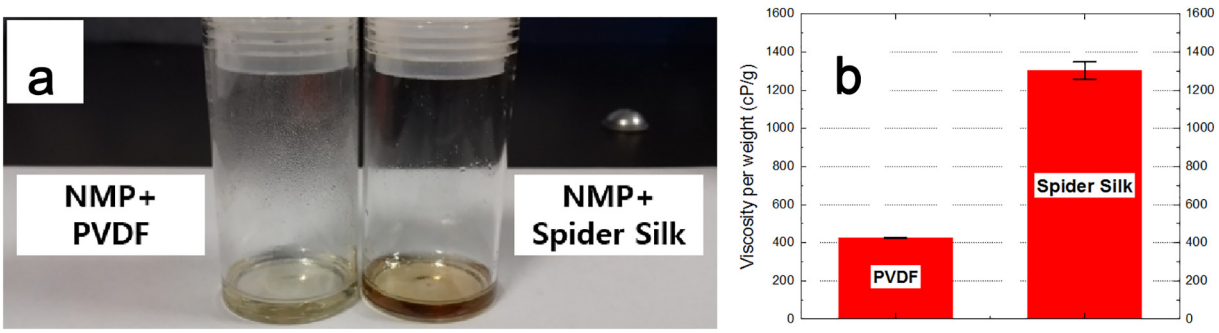

Fig. 5. (a) Color comparison of the color between the samples of NMP + PVDF and NMP + spider silk; (b) comparison of the viscosity per weight of PVDF and spider silk based binders. (For interpretation of the references to color in this figure, the reader is referred to the web version of this article.)

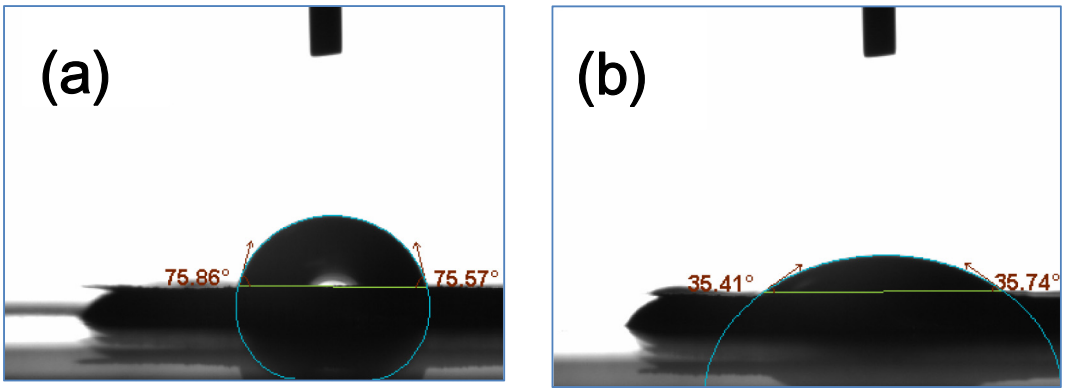

Fig. 6. Contact angle measurements of (a) SPVDF and (b) SWS based electrodes.

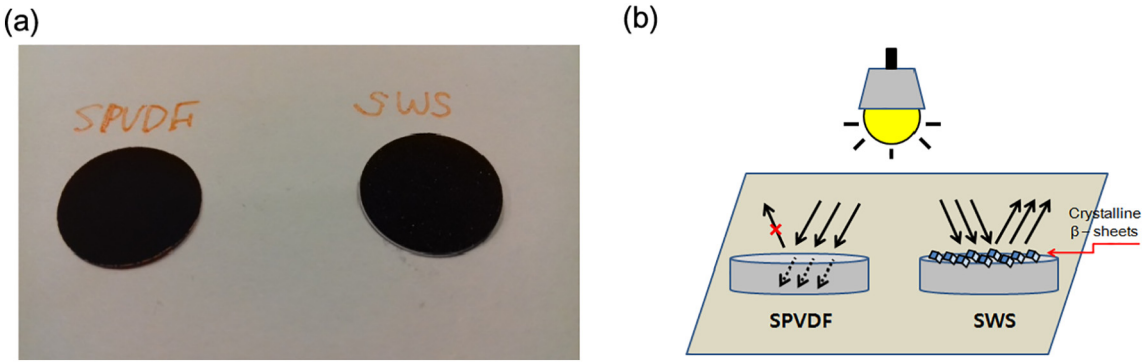

Fig. 7. (a) Comparison of surfaces of the SPVDF and the SWS electrodes with different binder materials; (b) A schematic diagram of the comparison of electrodes. (Note: A short movie file was also presented about this.)

Cyclic voltammetry (CV) was carried out in order to investigate the electrochemical behavior of the test electrodes. CV curves of the SWS and SPVDF based electrodes are shown in Fig. 8. The SPVDF curves are fairly similar to curves reported for crystalline Si electrodes with PVDF binder [38], and in the first cycle shows two broad cathodic (Li-insertion) peaks at 1.36 and 0.61 V, and two anodic (Li-extraction) peaks at 0.33 and 0.61 V. In the scan of Li-insertion, a less discernable peak at 1.36 V can be associated with the onset of solid electrolyte interface (SEI) layer formation [39], and the peak at 0.61 V attributed to the formation of the main SEI phase and electrolyte decomposition. These SEI peaks became indiscernible in the second cycle, which means that those reactions are irreversible. The current increase between 0.25 and 0.005 V for the cathodic peak is related to the conversion of Si to Li_xSi. In the scan of Li-extraction, two peaks at 0.33 and 0.61 V could be related to lithium de-alloying from Si.

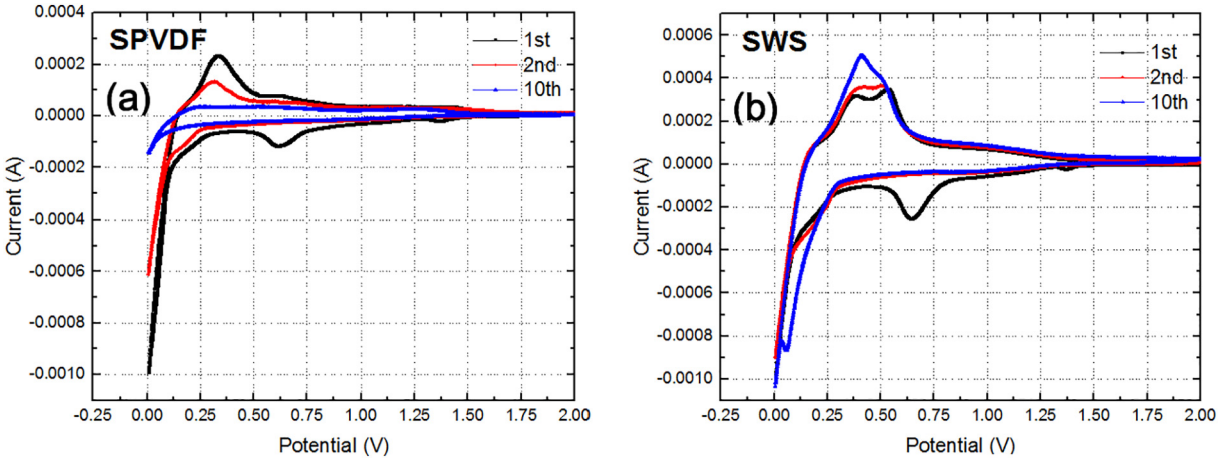

Fig. 8. Cyclic voltammograms between 0.005 and 2.0 V vs. Li/Li^+ at the scan rate of $0.1mVs^{-1}$ for silicon electrodes using: (a) SPVDF; (b) SWS binders.

These peaks gradually shifted to lower voltages and decreased in subsequent cycles, and finally disappeared in the 10th cycle. This implies that the kinetic process of Li-extraction no longer occurred. In the case of the SWS curves, cathodic peaks related to SEI formation and electrolyte decomposition are also observed at 1.36 and 0.64 V, respectively as shown in Fig. 8(b). Current peaks between 0.005 and 0.26 V, indicating the conversion of Si to Li_xSi phase, retained in subsequent cycles. Another peak at 0.05 V was displayed in the 10th cycle, and demonstrated the enhancement of the kinetic reaction in subsequent cycles. These results are different from those of SPVDF, and demonstrated the better cycling ability of SWS compared to SPVDF. In the anodic scan, peaks at 0.37 and 0.54 V are displayed in Fig. 8(b), and these would grow and finally converged at 0.41 V in subsequent cycles. This indicated that the reaction of Li-extraction changed. The cathodic peak at 0.05 V and the anodic peaks at 0.37 and 0.54 V are characteristic of amorphous Si [40]. The peak at 0.005 V indicates the reactions of crystalline or amorphous silicon, or both. In the first cathodic scan, only the crystalline Si reacted. Then, this structure would become amorphous during Li-insertion and two anodic peaks of amorphous Si are observed upon subsequent scans as shown in Fig. 8(b). The overall number of SPVDF peaks decreased in subsequent cycles, however, the number of SWS peaks would rise in cathodic scans and converged in anodic scans. This means that the Si electrode in SPVDF had separated from the electrode surface, and thus, the peaks are reduced with less reaction. However, the SWS electrode would continue to react with lithium ions due to the support provided by the stronger binder. Therefore, more varied curves are displayed in the repeated SWS cycles. These results indicated the positive effect of spider silk binder, which, in this respect, is superior to the commercial PVDF.

Electrochemical impedance spectroscopy (EIS) was carried out to analyze further the electrochemical behavior (i.e. charge transfer and ionic diffusion kinetics) of the electrodes. Fig. 9(a) shows the Nyquist plots and fitted curves of pristine SWS and SPVDF electrodes measured at open circuit voltage. Each plot exhibited a depressed semi-circle in the high frequency and a straight line in the low frequency range. This semi-circle is proportional to the charge transfer resistance (Rct). The slope of the line (Z′ against $\omega^{-1/2}$) is the Warburg factor of a Randles circuit, and it indicates the solid state diffusion of Li-ions inside the electrode [41,42]. The diffusion curves of SWS and SPVDF electrodes are clearly different as shown in Fig. 9(b). The lower slope of SWS indicates the reduced impedance of solid-state diffusion of Li-ions, and the Li-ion diffusion in SWS is much faster than in SPVDF. The SWS binder, which has much higher viscosity, may lead to a more cohesive particle network between the conductive agent and Si on the Cu-foil substrate. These results clearly support the improved performance and cyclic ability of SWS electrodes.

In order to further investigate the effect of spider silk as a binder, the electrochemical performance of Si-electrodes with SWS and SPVDF binders was measured. Fig. 10 presents the galvanostatic charge/discharge profiles of Si-electrodes a high current density of 250 mA g^{-1}. The SWS and SPVDF electrodes with weight ratio of 8:1.5:0.5 show the 1st discharge and charge capacities as 3061/820 and 3089/348 mAh g^{-1}. Then, their capacities were shown as 698/536 and 168/138 mAh g^{-1} at the 2nd cycle in Fig. 10(a) and (b). In the case of the weight ratio for 4.5:4.5:1, the SWS electrode showed the initial discharge/charge capacities of 3642/1938 mAh g^{-1} at 1st cycle, 1789/1541 mAh g^{-1} at 2nd cycle and then reduced to 1142/1054 mAh g^{-1} at the 5th cycle. However, the capacities of the SPVDF electrode were 3903/2694 mAh g^{-1}, 1455/1211 mAh g^{-1}, and 458/435 mAh g^{-1} (Fig. 10(c, d)). Fig. 10(e) shows the curve of cyclic performances of batteries with anodes using SWS and SPVDF binders, based on the results of figure (c, d).

The electrode with SWS exhibited superior cyclic performance, delivering a high reversible capacity. After the 1st cycle, the loss of large capacity is shown in SPVDF, and the capacity was almost lost within seven cycles. The discharge capacity exhibited 323 mAh g^{-1} at the 7th cycle. When compared to the cycling curve of SPVDF, that of SWS relatively retain its capacity. The capacity of SWS at the 38th cycle showed 333 mAh g^{-1}, which is still a higher number as compared with SPVDF. It indicated that the spider silk-based binder more efficiently suppress the volume expansion of Si than the PVDF binder. When all these results from the comparison between SWS and SPVDF were studied, it was clear that spider silk could contribute to enhanced cyclic ability of Si electrodes. Therefore, the unequivocal conclusion is that SWS is much more suitable as the binder for Li-ions batteries than SPVDF.

The SWS batteries exhibited better cycling performance and stability than the SPVDF based batteries. The results could be explained with the following possible reasons. One reason is the unique structure of the silks, consisting of crystal β-sheets and semi-amorphous structures. These structures are connected by covalent bonds, which ensure both strength and ductility.

Such bonds may support good electron-transport pathways and maintening the lattice constant, decreasing the ratio of the structural distortion, and leading to minimal pulverization of the Si-electrodes. Furthermore, the spread of crystal β-sheets could make folding-layer structures as shown in Fig. 11(b, c). The layered structure may provide fast and efficient intercalation and deintercalation of lithium (Li) ions,

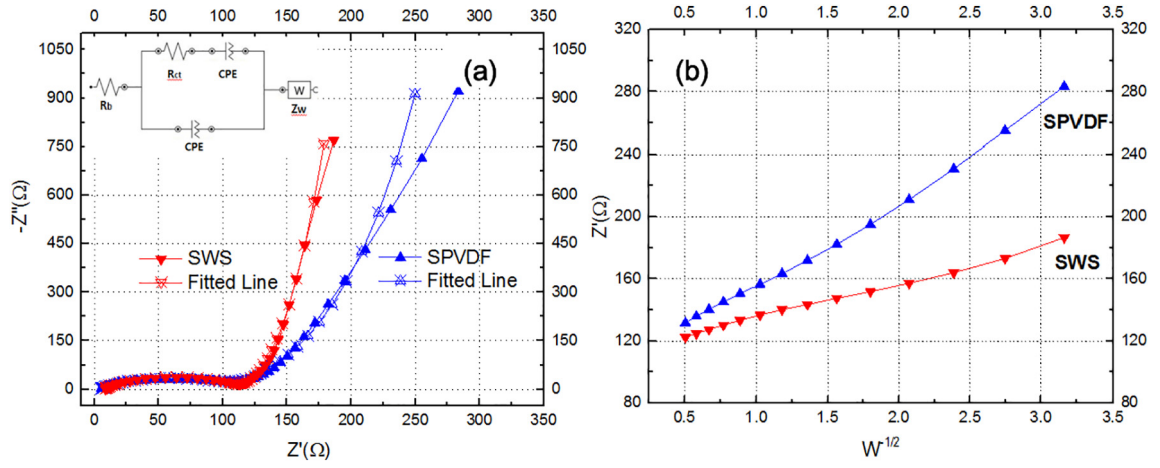

Fig. 9. Electrochemical impedance spectroscopy (EIS) spectra of SWS and SPVDF electrodes: (a) Nyquist plots (inset: equivalent circuit model); (b) relationship between Z′ and $\omega^{-1/2}$ in the low frequency region.

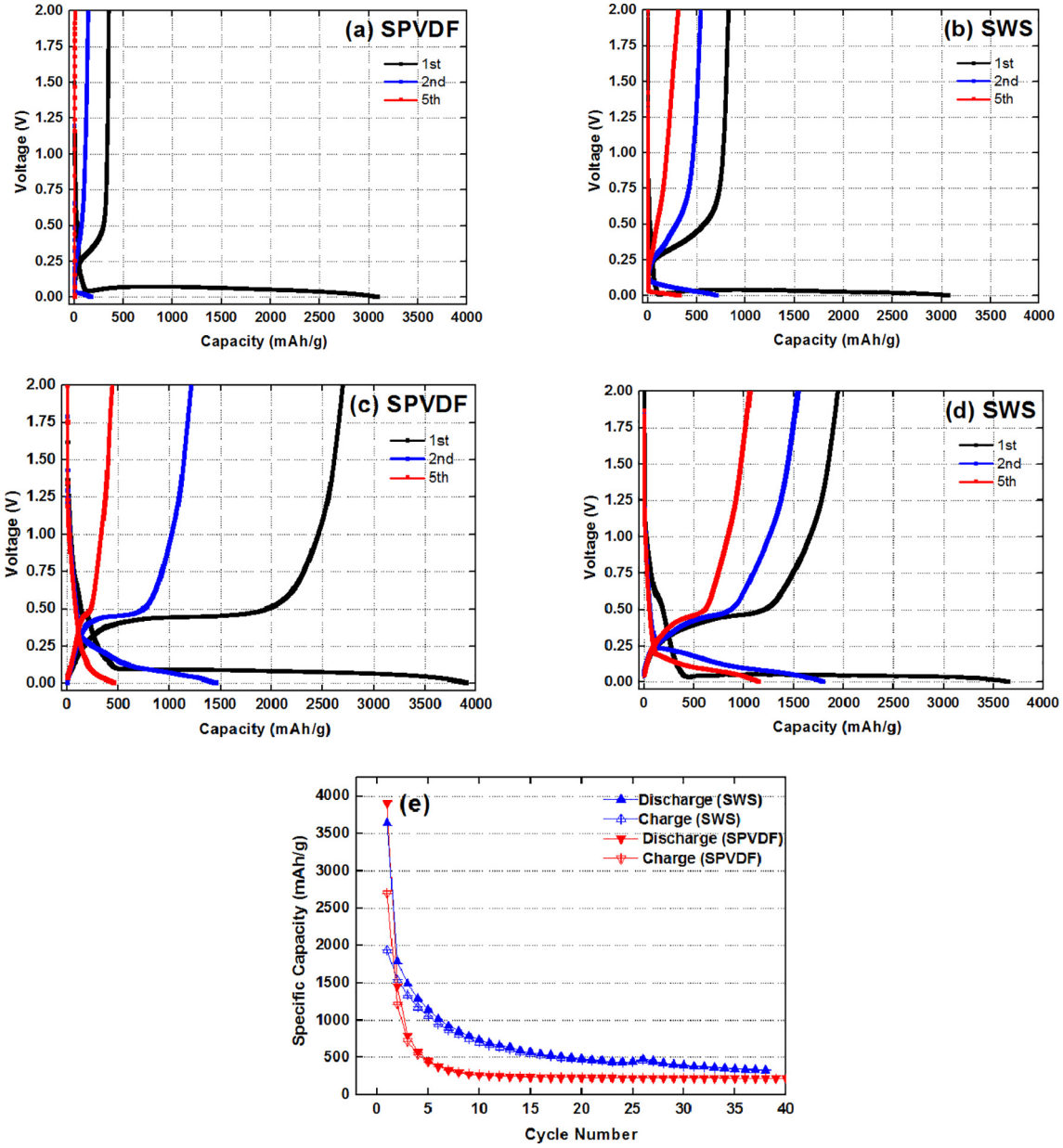

Fig. 10. Galvanostatic charge/discharge profiles of: (a) SPVDF and (b) SWS with the ratio of 8:1.5:0.5, and (c) SPVDF and (SWS) with the ratio of 4.5:4.5:1; (e)Cyclic performance for the SPVDF and SWS samples with the ratio of 4.5:4.5:1 at a high current density of 250 mA g^{-1} (the mass loading of Si in each electrode is (a) 2.12, (b) 3.74, (c) 0.32, and (d) 1.02 mg·cm^{-2}).

and thus provide facile accessibility of Li-ions during charge and discharge processes. This may cause an increased in the rate of Li-ion diffusion. The components in the silk, glycine and alanine can interact to allow a close packed stacking. The attractive forces between the glycine blocks and alanine blocks make it strong [43], and these may be related to the features of high viscosity and adhesion. From this interactive force, the β-sheets form tightly packed layers. These stacked sheets are linked with various bonds that add extra strength and this packing may minimize the volume expansion rate of the active materials. These bonds may play a role in restraining the volume change in the structure in the way that a spring may be compressed and stretched. The side chain R-groups of a crystal β-sheet (see Fig. 11) might change the properties of active materials to increase ion adsorption and hydrophilicity, which facilitate ion-transport into pores. These groups acted to provide enlarged surface area for promoting the electrochemical redox reactions, which might increase the amount of Li-ions stored in a battery. All the characteristics are advantageous in providing its superior performance and cycling stability.

4. Conclusions

This paper reported the novel approach of using natural spider silk as the effective binder material. The SWS based Li-ion cells showed superior capacities and cycling stability. The SWS electrode at 250 mA g^{-1} showed the discharge/charge capacities of 3642/1938 mAh g^{-1} at 1st cycle, 1789/1541 mAh g^{-1} at 2nd cycle and then reduced to 1142/1054 mAh g^{-1} at the 5th cycle. However, the capacities of the SPVDF electrode were 3903/2694 mAh g^{-1}, 1455/1211 mAh g^{-1}, and 458/435 mAh g^{-1}. Furthermore, the discharge capacity of SWS was 333 mAh/g at the 38th cycle, but that of SPVDF showed 323 mAh/g at only the 7th cycle, respectively. Such superior performance of SWS may be due to the unique properties of spider silk: the folded crystal layer

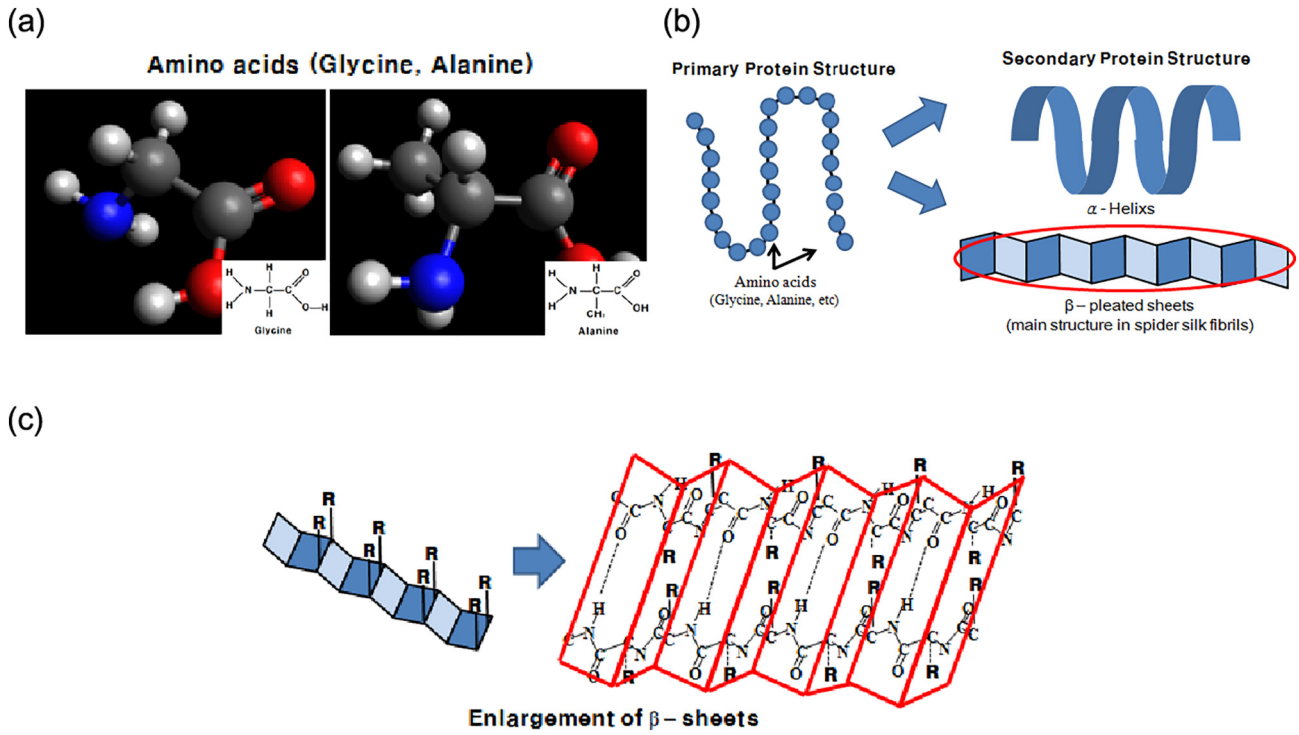

Fig. 11. (a) Chemical structure of two main components of amino acids in silk fibrils (Glycine and Alanine); (b) primary and secondary structures of proteins; (c) the enlargement of β-sheets.

with semi-amorphous structure, high viscosity and adhesion of the binder, and the close stacking by the proteins blocks, and the side chain R-group of crystal β-sheet. The combination of these characteristics may lead to the ability to significantly restrain the undesirable change in the volume of Si materials, and to provide superior electrochemical characteristics and performance of lithium ion batteries. The property of enhanced capacity with increased cycling stability in the SWS electrodes was demonstrated through cyclic voltammetry (CV), electrochemical impedance spectroscopy (EIS), and galvanostatic charge/discharge tests. These experimental results indicated that the use of spider silk inspired binder in Si electrode is a promising and novel approach to overcome the current severe problem of Si-volume expansion, thus enabling the practical application of Si-based anodes in Li-ion batteries. We expect that this study would also be helpful to understand the properties of spider silk materials and their potential usage as binders for supercapacitors and thermaelectrics.

Supplementary data to this article can be found online at https://doi.org/10.1016/j.matdes.2020.108669.

CRediT authorship contribution statement

DongWoong Choi: Conceptualization, Resources, Investigation, Writing - original draft.**Kwang-Leong Choy:**Conceptualization, Resources, Writing - review & editing, Supervision.

Declaration of competing interest

The authors declare that they have no known competing financial interests or personal relationships that could have appeared to influence the work reported in this paper.

Acknowledgement

The work is funded by UCL Institute for Materials Discovery.

References

[1] N. Liu, Z. Lu, J. Zhao, M.T. McDowell, H.-W. Lee, W. Zhao, Y. Cui, A pomegranate-inspired nanoscale design for large-volume-change lithium battery anodes, Nat. Nanotechnol. 9 (2014) 187.
[2] N. Yuca, M.F. Doğdu, M.E. Cetintasoglu, O.S. Taskin, I. Avci, Investigation of the Conductivity Effect on Silicon Anode Performance for Lithium Ion Batteries, Meeting Abstracts MA2016-02(3), 2016 275.
[3] I. Wolfram Research, Electrical conductivity of the elements, http://periodictable.com/Properties/A/ElectricalConductivity.an.html.
[4] Y. Jin, B. Zhu, Z. Lu, N. Liu, J. Zhu, Challenges and recent progress in the development of Si anodes for lithium-ion battery, Adv. Energy Mater. 7 (23) (2017), 1700715.
[5] J. Trinastic, Solving the silicon swelling problem in batteries, https://www.nature.com/scitable/blog/eyes-on-environment/solving_the_silicon_swelling_problem.
[6] X. Li, M. Gu, S. Hu, R. Kennard, P. Yan, X. Chen, C. Wang, M.J. Sailor, J.-G. Zhang, J. Liu, Mesoporous silicon sponge as an anti-pulverization structure for high-performance lithium-ion battery anodes, Nat. Commun. 5 (2014) 4105.
[7] L.-F. Cui, R. Ruffo, C.K. Chan, H. Peng, Y. Cui, Crystalline-amorphous core—shell silicon nanowires for high capacity and high current battery electrodes, Nano Lett. 9 (1) (2009) 491–495.
[8] C.K. Chan, H. Peng, G. Liu, K. McIlwrath, X.F. Zhang, R.A. Huggins, Y. Cui, High-performance lithium battery anodes using silicon nanowires, Nat. Nanotechnol. 3 (1) (2008) 31–35.
[9] J. Zhou, T. Qian, M. Wang, N. Xu, Q. Zhang, Q. Li, C. Yan, Core–shell coating silicon anode interfaces with coordination complex for stable lithium-ion batteries, ACS Appl. Mater. Interfaces 8 (8) (2016) 5358–5365.
[10] A. Magasinski, P. Dixon, B. Hertzberg, A. Kvit, J. Ayala, G. Yushin, High-performance lithium-ion anodes using a hierarchical bottom-up approach, Nat. Mater. 9 (4) (2010) 353–358.
[11] J. Ming, H. Ming, W.-J. Kwak, C. Shin, J. Zheng, Y.-K. Sun, The binder effect on an oxide-based anode in lithium and sodium-ion battery applications: the fastest way to ultrahigh performance, Chem. Commun. 50 (87) (2014) 13307–13310.
[12] G. Liu, H. Zheng, A.S. Simens, A.M. Minor, X. Song, V.S. Battaglia, Optimization of acetylene black conductive additive and PVDF composition for high-power rechargeable lithium-ion cells, J. Electrochem. Soc. 154 (12) (2007) A1129–A1134.
[13] J.-H. Lee, U. Paik, V.A. Hackley, Y.-M. Choi, Effect of poly(acrylic acid) on adhesion strength and electrochemical performance of natural graphite negative electrode for lithium-ion batteries, J. Power Sources 161 (1) (2006) 612–616.
[14] J. Chen, J. Liu, Y. Qi, T. Sun, X. Li, Unveiling the roles of binder in the mechanical integrity of electrodes for lithium-ion batteries, J. Electrochem. Soc. 160 (9) (2013) A1502–A1509.
[15] H.-K. Park, B.-S. Kong, E.-S. Oh, Effect of high adhesive polyvinyl alcohol binder on the anodes of lithium ion batteries, Electrochem. Commun. 13 (10) (2011) 1051–1053.

[16] M. Ko, S. Chae, J. Cho, Challenges in accommodating volume change of Si anodes for Li-ion batteries, ChemElectroChem 2 (11) (2015) 1645–1651.
[17] G.T. Kim, S.S. Jeong, M. Joost, E. Rocca, M. Winter, S. Passerini, A. Balducci, Use of natural binders and ionic liquid electrolytes for greener and safer lithium-ion batteries, J. Power Sources 196 (4) (2011) 2187–2194.
[18] A. Magasinski, B. Zdyrko, I. Kovalenko, B. Hertzberg, R. Burtovyy, C.F. Huebner, T.F. Fuller, I. Luzinov, G. Yushin, Toward efficient binders for Li-ion battery Si-based anodes: polyacrylic acid, ACS Appl. Mater. Interfaces 2 (11) (2010) 3004–3010.
[19] M. Manickam, M. Takata, Effect of cathode binder on capacity retention and cycle life in transition metal phosphate of a rechargeable lithium battery, Electrochim. Acta 48 (8) (2003) 957–963.
[20] C. Chen, S.H. Lee, M. Cho, J. Kim, Y. Lee, Cross-linked chitosan as an efficient binder for Si anode of Li-ion batteries, ACS Appl. Mater. Interfaces 8 (4) (2016) 2658–2665.
[21] I. Kovalenko, B. Zdyrko, A. Magasinski, B. Hertzberg, Z. Milicev, R. Burtovyy, I. Luzinov, G. Yushin, A major constituent of brown algae for use in high-capacity Li-ion batteries, Science 334 (6052) (2011) 75–79.
[22] S. Rammensee, U. Slotta, T. Scheibel, A.R. Bausch, Assembly mechanism of recombinant spider silk proteins, Proc. Natl. Acad. Sci. 105 (18) (2008) 6590–6595.
[23] J.L. Yarger, B.R. Cherry, A. van der Vaart, Uncovering the structure–function relationship in spider silk, Nat. Rev. Mater. 3 (3) (2018), 18008.
[24] C. Miceli, Spider Silk Is Five Times Stronger Than Steel—Now, Scientists Know Why, 2018.
[25] J.A. Kluge, O. Rabotyagova, G.G. Leisk, D.L. Kaplan, Spider silks and their applications, Trends Biotechnol. 26 (5) (2008) 244–251.
[26] Wikipedia, Hydrogen Bond, 2017 (Accessed January 10th 2017).
[27] sgorner, Spider Silk – Khamillah, http://gd-chemistry.boltonschool-senior.me/2014/02/26/spider-silk-khamillah/ 2014.
[28] C. Pigliacelli, A. D'Elicio, R. Milani, G. Terraneo, G. Resnati, F. Baldelli Bombelli, P. Metrangolo, Hydrophobin-stabilized dispersions of PVDF nanoparticles in water, J. Fluor. Chem. 177 (2015) 62–69.
[29] E. Shamsaei, M.M. Nasef, H. Saidi, A.H. Yahaya, Parametric investigations on proton conducting membrane by radiation induced grafting of 4-vinylpyridine onto poly (vinylidene fluoride) and phosphoric acid doping, Radiochim. Acta (2014) 351.
[30] K. Maji, R. Sarkar, S. Bera, D. Haldar, A small molecule peptidomimetic of spider silk and webs, Chem. Commun. 50 (84) (2014) 12749–12752.
[31] G.J.G. Davies, D.P. Knight, F. Vollrath, Chitin in the silk gland ducts of the spider Nephila edulis and the silkworm Bombyx mori, PLoS One 8 (8) (2013), e73225.
[32] N.A. Ibrahim, M, Kamal DE, Density functional theory and FTIR spectroscopic study of carboxyl group, Indian J. Pure Appl. Phys. 43 (12) (2005) 911–917.
[33] S.H.B.S. İde, T. Türkeş, Y. Orhan Mergen, Ö. Çelik, V. Bütün, M.F. Sargon, N. Kocatepe, M. Kriechbaum, Structural characterization of a variety of spider silks from Turkey using different biophysical techniques, J. Spectrosc. 25 (3–4) (2011) 155–167.
[34] P. Mohammadi, A.S. Aranko, C.P. Landowski, O. Ikkala, K. Jaudzems, W. Wagermaier, M.B. Linder, Biomimetic composites with enhanced toughening using silk-inspired triblock proteins and aligned nanocellulose reinforcements, Sci. Adv. 5 (9) (2019) eaaw2541.
[35] t.f.e. Wikipedia, Spider Silk.
[36] S.K.a.M.J. Buehler, Nanostructure and molecular mechanics of dragline spider silk protein assemblies, J. R. Soc. Interface (2010) 1709–1721.
[37] R. Hiesgen, S. Sörgel, R. Costa, L. Carlé, I. Galm, N. Cañas, B. Pascucci, K.A. Friedrich, AFM as an analysis tool for high-capacity sulfur cathodes for Li–S batteries, Beilstein J. Nanotechnol. 4 (2013) 611–624.
[38] J. Xu, Q. Zhang, Y.-T. Cheng, High capacity silicon electrodes with Nafion as binders for lithium-ion batteries, J. Electrochem. Soc. 163 (3) (2016) A401–A405.
[39] T. Zhang, J. Gao, H.P. Zhang, L.C. Yang, Y.P. Wu, H.Q. Wu, Preparation and electrochemical properties of core-shell Si/SiO nanocomposite as anode material for lithium ion batteries, Electrochem. Commun. 9 (5) (2007) 886–890.
[40] N. Liu, K. Huo, M.T. McDowell, J. Zhao, Y. Cui, Rice husks as a sustainable source of nanostructured silicon for high performance Li-ion battery anodes, Sci. Rep. 3 (2013) 1919.
[41] H. Gao, L. Jiao, W. Peng, G. Liu, J. Yang, Q. Zhao, Z. Qi, Y. Si, Y. Wang, H. Yuan, Enhanced electrochemical performance of LiFePO4/C via Mo-doping at Fe site, Electrochim. Acta 56 (27) (2011) 9961–9967.
[42] X. Liu, J. Zhang, W. Si, L. Xi, B. Eichler, C. Yan, O.G. Schmidt, Sandwich nanoarchitecture of Si/reduced graphene oxide bilayer nanomembranes for Li-ion batteries with long cycle life, ACS Nano 9 (2) (2015) 1198–1205.
[43] E.R. Gauthler, Biochemistry 1. http://slideplayer.com/slide/4556292/.